

# Self-Driven Photodetector and Ambipolar Transistor in Atomically Thin GaTe-MoS<sub>2</sub> p-n vdW Heterostructure

Shengxue Yang,<sup>†,‡</sup> Cong Wang,<sup>†,§,⊥</sup> Can Ataca,<sup>||</sup> Yan Li,<sup>#</sup> Hui Chen,<sup>#</sup> Hui Cai,<sup>△</sup> Aslihan Suslu,<sup>△</sup> Jeffrey C. Grossman,<sup>||</sup> Chengbao Jiang,<sup>\*,‡</sup> Qian Liu,<sup>\*,§,⊥</sup> and Sefaattin Tongay<sup>\*,△</sup>

<sup>‡</sup>School of Materials Science and Engineering, Beihang University, Beijing 100191, P.R. China

<sup>§</sup>The MOE Key Laboratory of Weak-Light Nonlinear Photonics, TEAD Applied Physics Institute and School of Physics, Nankai University, Tianjin 300457, China

<sup>⊥</sup>National Center for Nanoscience and Technology, No. 11 Beiyitiao, Zhongguancun, Beijing 100190, China

<sup>||</sup>Department of Materials Science and Engineering, Massachusetts Institute of Technology, Cambridge, Massachusetts 02139, United States

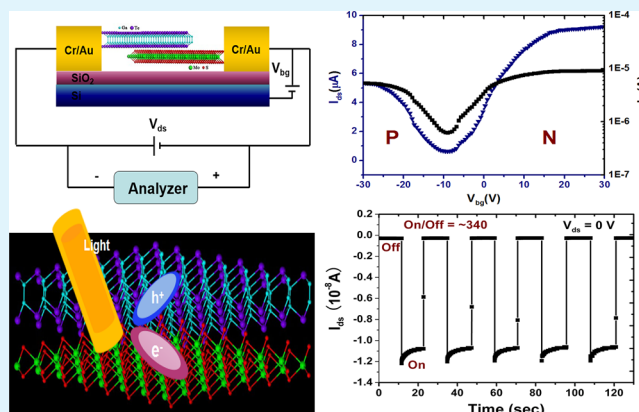
<sup>#</sup>State Key Laboratory of Superlattices and Microstructures, Institute of Semiconductors, Chinese Academy of Sciences, Beijing 100083, China

<sup>△</sup>School for Engineering of Matter, Transport and Energy, Arizona State University, Tempe, Arizona 85287, United States

## Supporting Information

**ABSTRACT:** Heterostructure engineering of atomically thin two-dimensional materials offers an exciting opportunity to fabricate atomically sharp interfaces for highly tunable electronic and optoelectronic devices. Here, we demonstrate abrupt interface between two completely dissimilar material systems, i.e., GaTe-MoS<sub>2</sub> p-n heterojunction transistors, where the resulting device possesses unique electronic properties and self-driven photoelectric characteristics. Fabricated heterostructure transistors exhibit forward biased rectifying behavior where the transport is ambipolar with both electron and hole carriers contributing to the overall transport. Under illumination, photoexcited electron-hole pairs are readily separated by large built-in potential formed at the GaTe-MoS<sub>2</sub> interface efficiently generating self-driven photocurrent within <10 ms. Overall results suggest that abrupt interfaces between vastly different material systems with different crystal symmetries still allow efficient charge transfer mechanisms at the interface and are attractive for photoswitch, photodetector, and photovoltaic applications because of large built-in potential at the interface.

**KEYWORDS:** self-driven photocurrent, ambipolar behavior, p-n heterojunction, rectification, dissimilar material systems



## INTRODUCTION

Unique properties of two-dimensional (2D) materials are appealing because they can extend electronics into new application realms.<sup>1</sup> Constructing well-defined heterostructures takes full advantages of their electronics.<sup>2</sup> Encouraged by the successful isolation of various 2D materials, designed heterostructures made by transferring one layered 2D material onto another and bonding through van der Waals (vdW) interactions have recently been investigated, revealing novel physical phenomena and distinctive capabilities.<sup>3,4</sup> For example, heterostructures of MoS<sub>2</sub> and WSe<sub>2</sub> have exhibited excellent rectification behavior, prominent electroluminescence, and strong interlayer coupling.<sup>5-7</sup> Graphene/MoS<sub>2</sub> heterostructures demonstrate large hysteresis in transport characteristics, high field effect on-off current ratio, gated-tunable persistent photoconductivity, as well as a large memory window and

stable retention.<sup>8-10</sup> Robust superlubricity and tunable plasmonics in graphene/h-BN heterostructures have also been explored.<sup>11</sup>

Heterostructures based on 2D layered materials exhibit four important features: (1) their atomically thin thickness, which is useful for efficient electrostatic tuning of the carrier densities, providing a relatively easy method to design complex functional devices;<sup>12,13</sup> (2) an intrinsic surface free of dangling bonds and weak vdW interaction enabling 2D layered materials to create the high-quality heterojunctions without the constraints of lattice mismatch;<sup>4,5,7</sup> (3) charge transport time and distance shortened by layered heterostructures resulting in enhancement

Received: October 20, 2015

Accepted: January 12, 2016

Published: January 12, 2016

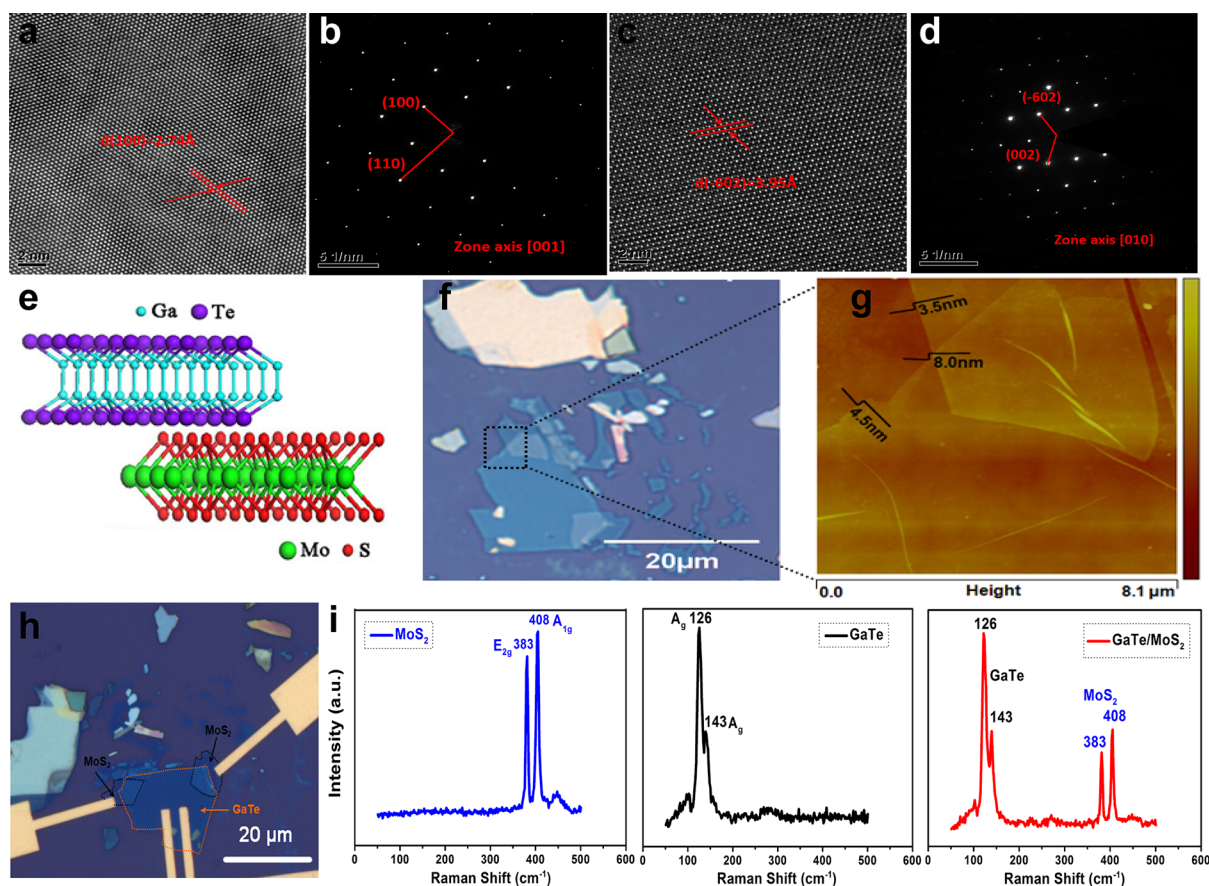


**Figure 1.** (a, c) TEM images of individual MoS<sub>2</sub> and individual GaTe, the scale bar is 2 nm, (b, d) corresponding SAED patterns of individual MoS<sub>2</sub> and individual GaTe. (e) Schematic of a GaTe-MoS<sub>2</sub> heterostructure. (f) Optical microscope image and (g) the selected region of AFM image of a GaTe-MoS<sub>2</sub> p-n heterostructure. (h) Optical microscope image of the vertical stacked GaTe-MoS<sub>2</sub> p-n heterostructural transistors. (i) Room-temperature Raman spectra for the different positions on the sample: individual MoS<sub>2</sub> (blue), individual GaTe (black), and the GaTe-MoS<sub>2</sub> heterostructures (red). The wavelength of the laser used is 514 nm.

of photoelectrochemical activity;<sup>14</sup> and (4) strong light-matter interactions that enhance the photon absorption and electron-pair creation, providing the possibility of optoelectronic devices with layered heterostructures.<sup>7,15</sup>

Vertical 2D heterostructures have already been utilized to create high-performance field effect transistors (FETs), photodiodes, photovoltaic cells, barristors, inverters, LEDs, sensors, and memory devices.<sup>5,6,8-10,16,17</sup> The differences of atomically thin 2D materials in their work functions, band gaps, and spin-orbit coupling strengths allow for a variety of useful heterojunction properties.<sup>18</sup> Type-II heterostructures of 2D materials are formed by careful band alignment engineering and material selection, provide an ideal platform for facilitating efficient photoexcited electron-hole separation for optoelectronic and light-harvesting applications.<sup>7,15,18,19</sup> These type II heterojunctions present ultrafast charge transfer, tuning interlayer coupling, and high interface recombination current.<sup>15,20-23</sup> With the introduction of these heterostructures, a p-n junction at the ultimate quantum limit is also realized and exhibits completely different transport characteristics than bulk junctions. The p-n vdW heterojunctions serve as the basic building blocks of modern optoelectronic devices exhibiting high photovoltaic response, well-defined current rectification, prominent band edge excitonic emission and enhanced hot electron luminescence.<sup>2,6,7,10,17</sup> Considering the great variety of 2D layered materials, further exploration of layered vdW

heterostructures with superior properties and functions is of great significance.

In this work, we report on heterostructures of 2D materials from different material systems: MoS<sub>2</sub>, a 1.3 eV indirect gap layered semiconductor with few-layered structure from the transition metal dichalcogenide (TMDs) family and GaTe, a 1.7 eV direct gap semiconductor from the post-transition metal chalcogenide (PTMCs) family. Intrinsically, MoS<sub>2</sub> shows high crystal symmetry and is an n-type semiconducting 2D material with hexagonal layered structure where the covalently bonded S-Mo-S sandwiched layers are bound by weak vdW forces (Figure 1a).<sup>24</sup> GaTe, however, is a p-type semiconductor with a less symmetric monoclinic structure in which two different Ga-Ga bonds exist in a single layer (as shown in Figure 1c), with the in-plane anisotropic characteristics of GaTe responsible for its different properties.<sup>12,25</sup> Fabricated GaTe-MoS<sub>2</sub> p-n heterostructure transistors exhibit ambipolar behavior with both electron and hole carriers contributing to the overall transport. Under illumination, self-driven photocurrent is also efficiently generated within <10 ms because of the effective separation of electron-hole pairs caused by large built-in potential and type II band alignment formed at the GaTe-MoS<sub>2</sub> interface.

Our team grew MoS<sub>2</sub> crystals using conventional vapor transport technique in a two-zone furnace and GaTe crystals by vertical Bridgman technique. Typical growth process yielded ~0.7–1.4 cm in size highly crystalline pieces. Transmission electron microscope (TEM) studies and diffraction patterns

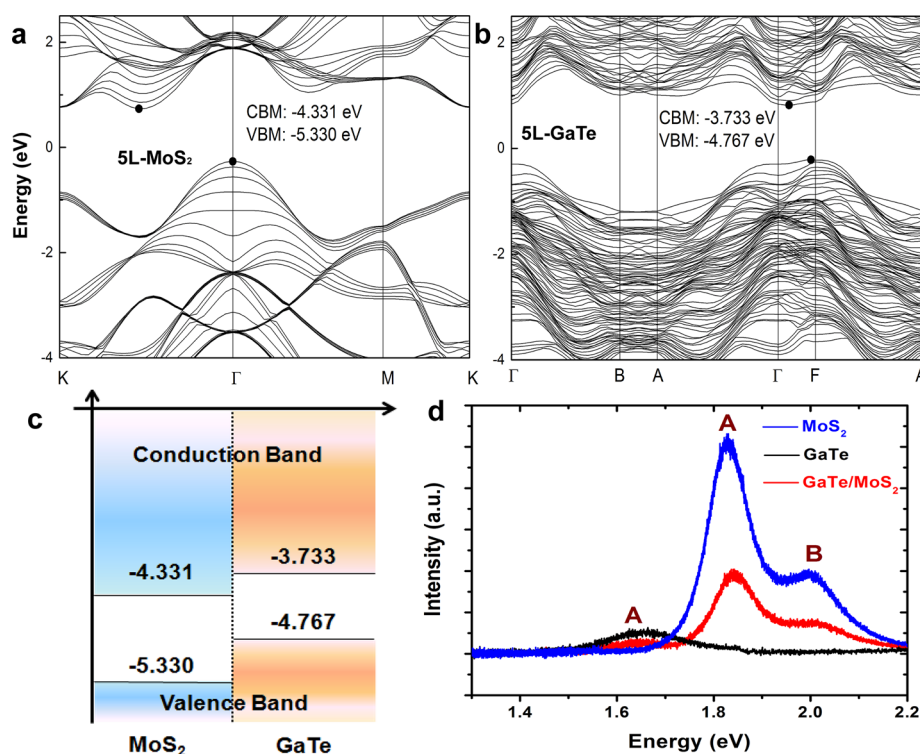


**Figure 2.** (a, b) Calculated band structures of individual MoS<sub>2</sub>, individual GaTe (monoclinic structure), respectively. (c) Schematic of the theoretically predicted band alignment of the GaTe-MoS<sub>2</sub> heterostructure, forming a type-II structure. (d) Photoluminescence spectra measured at different positions of the sample under 514 nm laser excitation: individual MoS<sub>2</sub> (blue), individual GaTe (black), and the GaTe-MoS<sub>2</sub> heterostructures (red).

confirmed the atomic structures and crystallinity of the MoS<sub>2</sub> and GaTe crystals (Figure 1a–d). The corresponding selected area electron diffraction (SAED) patterns indicate that the layered 2H-MoS<sub>2</sub> belongs to a hexagonal crystal system (JCPDS 37–1492) oriented along (001) zone axis and monoclinic GaTe oriented along (010) zone axis, corresponding to the PDF card (JCPDS 44–1127), as shown in Figure 1b, d. The vertically stacked heterojunction transistor (Figure 1e) was formed by transferring p-type GaTe onto exfoliated n-type MoS<sub>2</sub> flakes using dry stamping technique with poly(methyl methacrylate) (PMMA) polymer serving as a transfer mediator. An example heterostructure with 4-terminal Cr/Au leads is shown in Figure 1h. We fabricated Cr/Au (8 nm/50 nm) electrodes by electron-beam lithography (EBL) followed by an electron beam evaporation (EBE) used as an electrical contact (see Figure S1 for detailed fabrication process of the heterojunction device).

We confirmed the presence of MoS<sub>2</sub>/GaTe heterojunctions using micro-Raman spectroscopy measurements (Figure 1i). For individual MoS<sub>2</sub>, the observed typical peaks at 383 and 408 cm<sup>-1</sup> attribute to the in-plane E<sub>2g</sub><sup>1</sup> phonon mode and the out-of-plane A<sub>1g</sub> mode, respectively.<sup>2,15,17</sup> The micro-Raman spectrum from individual GaTe has two peaks at 126 and 143 cm<sup>-1</sup>, in agreement with the A<sub>g</sub> modes of GaTe (Γ point phonons).<sup>25</sup> The micro-Raman peaks of GaTe-MoS<sub>2</sub> heterostructure demonstrate the representative vibration modes of both GaTe and MoS<sub>2</sub> indicating the coexistence of two distinct materials within the heterostructure.

To elucidate the band alignment and charge transfer in the GaTe-MoS<sub>2</sub> heterostructure, we performed first-principle calculations and photoluminescence (PL) spectra on GaTe-MoS<sub>2</sub> heterostructure samples. According to the atomic force

microscopy (AFM) measurement (Figure 1f, g), the thickness of MoS<sub>2</sub> and GaTe are ~3.5 and ~4.5 nm, corresponding to five-layer samples, respectively,<sup>12,24</sup> and thus we performed our DFT calculations for five-layer MoS<sub>2</sub> and five-layer GaTe to simulate the heterojunctions accurately. Our band structure results, in Figure 2a–b, and their valence band maximum (VBM) and conduction band minimum (CBM) values summarized in Figure 2c, show that GaTe-MoS<sub>2</sub> p–n heterojunctions form type II heterolayers.<sup>26</sup> The DFT calculations are smaller than our experimentally observed values as DFT within generalized gradient approximation and local density approximation usually underestimates the band gap to a large degree.<sup>27</sup> Figure 2d displays typical PL spectra for GaTe-MoS<sub>2</sub> heterostructure, individual MoS<sub>2</sub> and individual GaTe under 514 nm laser excitation. Under strong laser intensity, individual MoS<sub>2</sub> shows mild PL signals of both A excitonic peak at 1.8 eV and B excitonic peak at 2.0 eV. Here we note that 1.4 eV peak associated with the indirect gap band of five-layer MoS<sub>2</sub> could not be observed possibly because of strong laser excitation induced hot luminescence (A and B excitons) peaks dominating over 1.4 eV peak, defects assisted weakening of phonon assisted indirect emission process, or turbostatic interlayer coupling influencing the CBM and VBM in such a way to halt indirect emission line. Similarly, GaTe flakes have an emission line at 1.65 eV, which is related to hot luminescence from few-layer flakes.<sup>28</sup> At the heterojunction (overlapped) area, all peaks appear at 1.65, 1.8, and 2.0 eV, but their intensities are quenched due to ultrafast charge transfer process consistent with earlier results on MoS<sub>2</sub>–WS<sub>2</sub> type II heterojunctions.<sup>7,15</sup> For the magnified PL spectra measured at different positions of the sample see Figure S2.

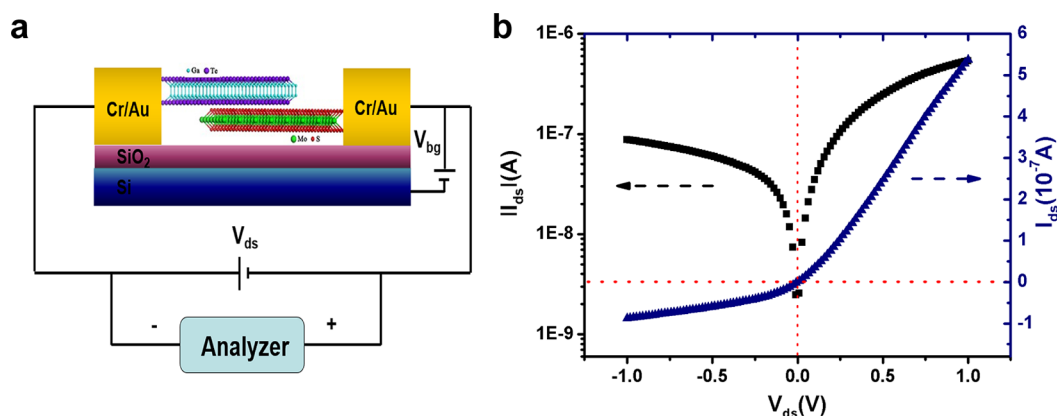


**Figure 3.** (a) Schematic diagram of the GaTe-MoS<sub>2</sub> heterostructure transistors. (b) Current–voltage curve of the device ( $V_{ds} = -1$  to  $1$  V,  $V_{bg} = 0$  V).

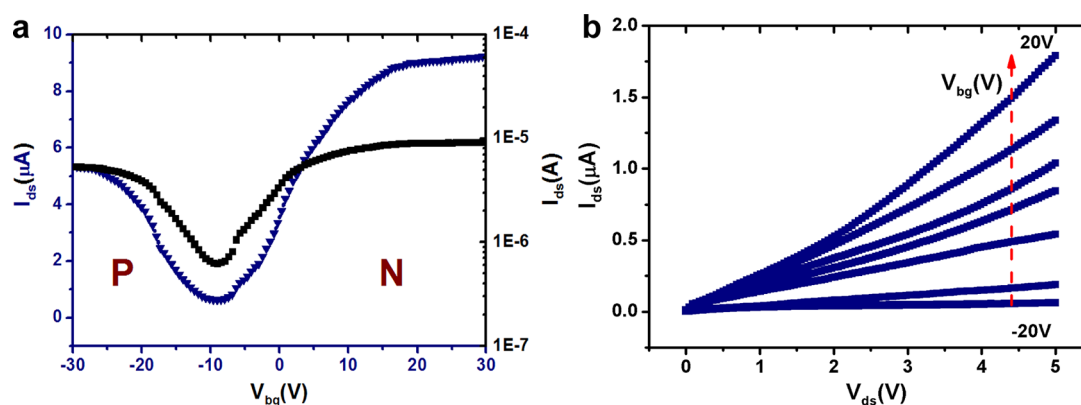


**Figure 4.** (a) Transfer characteristics of GaTe-MoS<sub>2</sub> heterostructure transistors measured with positive source drain voltage ( $V_{ds} = 15$  V,  $V_{bg} = -30$ – $30$  V), (b) output characteristics of GaTe-MoS<sub>2</sub> heterostructure transistors measured with positive  $V_{ds}$  ( $V_{ds} = 0$ – $5$  V,  $V_{bg} = -20$  to  $20$  V).

Figure 3a shows a GaTe-MoS<sub>2</sub> p–n junction transistor schematic and typical measurement setup. All electrical transport measurements were completed under ambient conditions at room temperature. Prior to measuring p–n transistor performance, we tested the contacts to MoS<sub>2</sub> and GaTe on Au/Cr/MoS<sub>2</sub> and Au/Cr/GaTe junctions separately using linear  $I$ – $V$  characteristics (Figure S3, black lines).<sup>6</sup> It is noted that better contact resistance and ohmic behavior for the device are helpful to the improvement of the current values. Transfer and output characteristics shown in Figures S4–S6 show that the current increased with rising positive gate voltage for MoS<sub>2</sub>, demonstrating an n-type behavior<sup>2,24</sup> and increased for GaTe with rising negative gate voltage, indicating a p-type behavior.<sup>27</sup> Large built-in potential formed at the GaTe-MoS<sub>2</sub> interface associated with large charge transfer across the interface.  $I$ – $V$  characteristics of the vertical GaTe-MoS<sub>2</sub> heterostructure exhibits typical forward bias rectifying behavior with an on–off current ratio of about 10 (Figure 3b).<sup>29</sup> Under a positive bias voltage, the built-in potential at the interface between GaTe and MoS<sub>2</sub> was much reduced, and the electrons easily transported across the layers, resulting in large on-state current. Similarly, under a negative bias voltage, the built-in potential was much greater and resulted in small off-state current.

Regarding the transfer characteristics of the heterostructure transistors (Figure 4a), the source-drain current ( $I_{ds}$ ) is recorded as constant source-drain bias ( $V_{ds}$ ), whereas Si substrate serves as a back gate.  $I_{ds}$  is strongly modulated by

the change of back-gate voltage ( $V_{bg}$ ), which is swept from negative to positive voltage. As indicated in Figure 4a, when the positive  $V_{ds}$  ( $V_{ds} = 15$  V) was applied, a nonmonotonic p–n ambipolar transport could be observed, which was associated with both electrons and holes contributing to the overall conductivity and with slightly large electron conductivity over hole.<sup>29</sup> It is worth noting that except for the rectifying behaviors, the GaTe-MoS<sub>2</sub> heterostructure transistors also exhibited the ambipolar characteristics; this is different from some heterojunction devices fabricated from the same material systems showing single polarity.<sup>6</sup> We also note that previous studies have demonstrated similar ambipolar responses on different material systems in similar bias ranges.<sup>29,30</sup> As presented in Figure 4a, we calculated the field effect mobility of GaTe-MoS<sub>2</sub> heterostructure transistors using the equation  $\mu = [dI_{ds}/dV_{bg}][L/(WC_1V_{ds})]$ , where  $C_1 = 1.15 \times 10^{-4}$  F m<sup>-2</sup> is the capacitance per unit area between the conducting channel and the back gate.<sup>27</sup> The calculated field-effect mobility of hole for p-type part of transfer curve in Figure 4a is determined to be  $1.8$  cm<sup>2</sup> V<sup>-1</sup> s<sup>-1</sup>, and the mobility of electron for n-type part is  $3.3$  cm<sup>2</sup> V<sup>-1</sup> s<sup>-1</sup>, slightly bigger than its p-type part. It is worth mentioning that the above equation assumes that either  $V_{ds}$  does not cause large spatial carrier density variation or electronic mobility is essentially independent from the carrier density. We argue that this assumption largely holds for 2D and quasi-2D heterogeneous junctions as scattering in 2D is mostly dominated by electron–phonon and Coulomb scattering effects (due to dielectric screening). Thus, variation in the

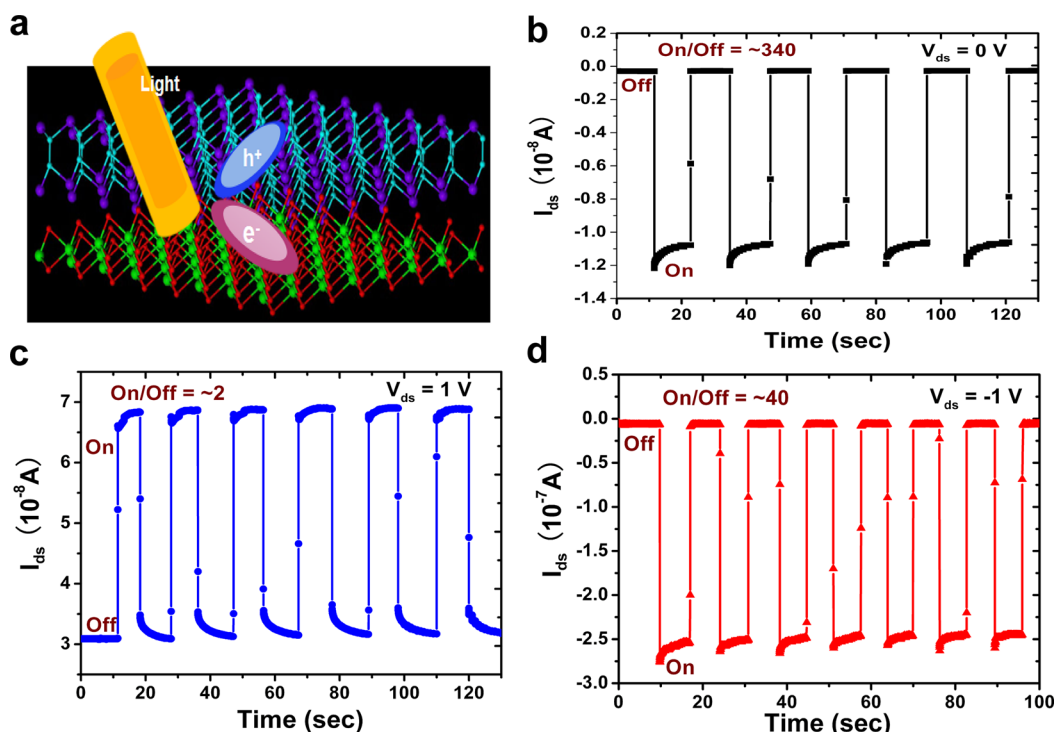


**Figure 5.** (a) Schematic diagram of the high-efficiency photoexcitons separation process. (b) Self-driven photoswitch behavior of GaTe-MoS<sub>2</sub> heterostructure photodetector ( $V_{ds} = 0$  V). Time dependences of source drain current curves under (c) positive bias voltage ( $V_{ds} = 1$  V) and (d) negative bias voltage ( $V_{ds} = -1$  V).

carrier density, if there is any significant change, does not influence the mobility substantially and above equation is valid for order of magnitude estimation. Contrary to the unipolarity of the individual constituents, this ambipolar behavior is due to both p-type GaTe constituent and n-type MoS<sub>2</sub> constituent existing in the same heterostructure system (Figures S4 and S5). In the transfer curve (Figure 4a), when the  $V_{bg} < -10$  V, then gate-induced holes in GaTe play a major role and contribute to the p-type electrical conductivity of the heterostructure. Conversely, the electrons in MoS<sub>2</sub> cause the n-type behavior under condition of  $V_{bg} > -10$  V. The output characteristics under different  $V_{bg}$  show that the output current changes simultaneously with increasing positive  $V_{ds}$  values (Figure 4b).

We also examined the photoswitch characteristics of the MoS<sub>2</sub>/GaTe heterostructure photodetectors under irradiation by a 633 nm laser excitation. Figure 5 shows the time dependence of source drain current  $I_{ds}$  at different source-drain bias voltage  $V_{ds}$  under light illumination. When  $V_{ds}$  was set to 0 V,  $I_{ds}$  changed rather quickly within <10 ms (Figure S7) by repetitive switching on–off the laser source, indicating good stability and repeatability of GaTe-MoS<sub>2</sub> heterostructure. This heterostructure shows a photoswitch property with photocurrent on–off ratio reaching ~340, higher than that observed in individual GaTe (on–off ratio ~10) and individual MoS<sub>2</sub> (on/off ratio ~85), as shown in Figures S3 and S5. From the time dependence of photoresponse with  $V_{ds}$  of 1 V (Figure 5c), the photocurrent quickly changed between on and off states with a photoswitch on–off ratio of ~2. However, the photoswitch on–off ratio under negative bias voltage ( $V_{ds} = -1$  V) was much larger than that obtained at positive bias voltage (Figure 5d). When we measured the optoelectronic performance of our GaTe-MoS<sub>2</sub> heterostructure devices, the applied bias voltage is zero. Under light illumination, a large

number of electron–hole pairs were generated. Because the type II band alignment and the existence of built-in potential in the p–n heterojunction, the photogenerated electron–hole pairs can be efficiently separated (Figure 5a). The electrons and holes respectively accumulated in MoS<sub>2</sub> and GaTe, resulting in the formation of open-circuit voltage. The built-in potential drove the photogenerated electrons and holes when the heterojunction operated under short-circuit condition, which produced the short-circuit current and resulted in the highly efficient electron–hole separation and self-driven photoswitch.

The photoresponsivity ( $R_\lambda$ ) and external quantum efficiency (EQE) are both critical parameters for photoswitch, which determines sensitivity for an optoelectronic device.<sup>31</sup>  $R_\lambda$  and EQE can be calculated in the following equations:  $R_\lambda = \Delta I_\lambda / (P_\lambda S)$  and  $EQE = hcR_\lambda / (e\lambda)$ , where  $\Delta I_\lambda = I_{\text{light}} - I_{\text{dark}}$  is the photocurrent,  $P_\lambda$  (100 mW cm<sup>-2</sup>) is the incident light intensity,  $S$  is the effective illuminated area,  $h$  is Planck's constant,  $c$  is the light velocity,  $e$  is the electronic charge, and  $\lambda$  (633 nm) is the incident light wavelength.<sup>12,32,33</sup> Here, we note that typically this method is usually applicable to the optoelectronic devices, such as photodetectors and photodiodes, as exemplified by recent literature.<sup>34–41</sup> Table 1 lists the performance comparison

**Table 1.** Photoresponse Parameter Comparison of Our p–n Photodetectors to Other Devices

	$R_\lambda$ (AW <sup>-1</sup> )	EQE (%)	response time
our p-n photodetectors	1.365	266	<10 ms
MoS <sub>2</sub> /Si p–n diodes <sup>42</sup>		4.4	
carbon nanotube-MoS <sub>2</sub> p–n diode <sup>31</sup>	0.1	25	<15 $\mu$ s
MoS <sub>2</sub> photodetectors <sup>44</sup>	880		4 s
MoS <sub>2</sub> device <sup>45</sup>	0.25–4.1		2 s

of our GaTe-MoS<sub>2</sub> heterostructure to other reported optoelectronic devices. The calculated  $R_{\lambda}$  and EQE of our GaTe-MoS<sub>2</sub> heterostructure photodetector under 0 V bias voltage are 1.36 A W<sup>-1</sup> and 266%, respectively, which are higher than the monolayer MoS<sub>2</sub>/Si p-n diodes;<sup>42</sup> however, the response is less sensitive than the carbon nanotube-MoS<sub>2</sub> heterojunction p-n diode and another vdW heterostructure device.<sup>32,43</sup> Thus, our GaTe-MoS<sub>2</sub> heterostructures prove useful for the highly efficient self-driven photodetectors, sensitive photoswitches, and some photovoltaic devices.

## CONCLUSION

In summary, using GaTe and MoS<sub>2</sub> from different material systems, we have fabricated atomically thin GaTe-MoS<sub>2</sub> p-n heterojunctions coupled by vdW forces. The GaTe-MoS<sub>2</sub> p-n heterojunctions possessed both distinctive transport and excellent photoresponse, producing better electronic and optoelectronic properties than their individual constituents. The transfer characteristic of our device showed a first decline then rising curve, indicating a p-n ambipolar behavior which differed from some heterojunction devices based on the 2D materials from the same system. These heterostructures exhibited a self-driven photocurrent with high on-off ratio at 0 V bias voltage under illuminating. We attributed this to the efficient electron-hole separation induced by built-in potential and type II band alignment. The photoresponse and EQE of the heterojunction were 1.36 A W<sup>-1</sup> and 266%, respectively. We expected all observed novel performances of the GaTe-MoS<sub>2</sub> p-n heterostructures, utilizing atomically thin 2D heterostructures from different material systems, to provide a promising route for future electronic and optoelectronic devices.

## ASSOCIATED CONTENT

### Supporting Information

The Supporting Information is available free of charge on the ACS Publications website at DOI: 10.1021/acsami.5b10001.

Detailed experimental process and Figures S1–S7 (PDF)

## AUTHOR INFORMATION

### Corresponding Authors

\*E-mail: jiangcb@buaa.edu.cn.

\*E-mail: liuq@nanocr.cn.

\*E-mail: sefaattin.tongay@asu.edu.

### Author Contributions

<sup>†</sup>S.Y. and C.W. contributed equally to this work. S.Y. and C.W. worked on device fabrication and performed the measurements. S.Y. and S.T. analyzed the data. H.C., Y.L., C.A., and J.G. performed simulation calculations. A.S., H.C., and S.T. synthesized the MoS<sub>2</sub> and GaTe crystals. S.T., C.J., and Q.L. discussed the experiments in this work. S.Y., C.J., and S.T. wrote the manuscript. All the authors read and commented on the manuscript.

### Notes

The authors declare no competing financial interest.

## ACKNOWLEDGMENTS

This work is supported by the National Natural Science Foundations of China (NSFC) under Grant 51331001. Q.L. acknowledges the support to this work by NSFC (10974037), NBRPC (2010CB934102), and the CAS Strategy Pilot

program (XDA 09020300). S.T. acknowledges Arizona State University Seeding Funding.

## REFERENCES

- (1) Yu, L.; Lee, Y.; Ling, X.; Santos, E. J. G.; Shin, Y. C.; Lin, Y.; Dubey, M.; Kaxiras, E.; Kong, J.; Wang, H.; Palacios, T. Graphene/MoS<sub>2</sub> Hybrid Technology for Large-Scale Two-Dimensional Electronics. *Nano Lett.* **2014**, *14*, 3055–3063.
- (2) Duan, X.; Wang, C.; Shaw, J. C.; Cheng, R.; Chen, Y.; Li, H.; Wu, X.; Tang, Y.; Zhang, Q.; Pan, A.; Jiang, J.; Yu, R.; Huang, Y.; Duan, X. Lateral Epitaxial Growth of Two-dimensional Layered Semiconductor Heterojunctions. *Nat. Nanotechnol.* **2014**, *9* (12), 1024–1030.
- (3) Geim, A. K.; Grigorieva, I. V. Van Der Waals Heterostructures. *Nature* **2013**, *499*, 419–425.
- (4) Kang, J.; Li, J.; Li, S.; Xia, J.; Wang, L. Electronic Structural Moiré Pattern Effects on MoS<sub>2</sub>/MoSe<sub>2</sub> 2D Heterostructures. *Nano Lett.* **2013**, *13* (11), 5485–5490.
- (5) Roy, T.; Tosun, M.; Kang, J. S.; Sachid, A. B.; Desai, S. B.; Hettick, M.; Hu, C. C.; Javey, A. Field-Effect Transistors Built from All Two-Dimensional Material Components. *ACS Nano* **2014**, *8* (6), 6259–6264.
- (6) Cheng, R.; Li, D.; Zhou, H.; Wang, C.; Yin, A.; Jiang, S.; Liu, Y.; Chen, Y.; Huang, Y.; Duan, X. Electroluminescence and Photocurrent Generation from Atomically Sharp WSe<sub>2</sub>/MoS<sub>2</sub> Heterojunction p-n Diodes. *Nano Lett.* **2014**, *14*, 5590–5597.
- (7) Lee, C.; Lee, G.; van der Zande, A. M.; Chen, W.; Li, Y.; Han, M.; Cui, X.; Arefe, G.; Nuckolls, C.; Heinz, T. F.; Guo, J.; Hone, J.; Kim, P. Atomically Thin p-n Junctions with Van Der Waals Heterointerfaces. *Nat. Nanotechnol.* **2014**, *9* (9), 676–681.
- (8) Roy, K.; Padmanabhan, M.; Goswami, S.; Sai, T. P.; Ramalingam, G.; Raghavan, S.; Ghosh, A. Graphene–MoS<sub>2</sub> Hybrid Structures for Multifunctional Photoresponsive Memory Devices. *Nat. Nanotechnol.* **2013**, *8*, 826–830.
- (9) Choi, M. S.; Lee, G.; Yu, Y.; Lee, D.; Lee, S. H.; Kim, P.; Hone, J.; Yoo, W. J. Controlled Charge Trapping by Molybdenum Disulphide and Graphene in Ultrathin Heterostructured Memory Devices. *Nat. Commun.* **2013**, *4*, 1624.
- (10) Yu, W. J.; Li, Z.; Zhou, H.; Chen, Y.; Wang, Y.; Huang, Y.; Duan, X. Vertically Stacked Multi-heterostructures of Layered Materials for Logic Transistors and Complementary Inverters. *Nat. Mater.* **2013**, *12*, 246–252.
- (11) Leven, I.; Krepel, D.; Shemesh, O.; Hod, O. Robust Superlubricity in Graphene/h-BN Heterojunctions. *J. Phys. Chem. Lett.* **2013**, *4*, 115–120.
- (12) Wang, Z.; Xu, K.; Li, Y.; Zhan, X.; Safdar, M.; Wang, Q.; Wang, F.; He, J. Role of Ga Vacancy on a Multilayer GaTe Phototransistor. *ACS Nano* **2014**, *8* (5), 4859–4865.
- (13) Yu, W. J.; Liu, Y.; Zhou, H.; Yin, A.; Li, Z.; Huang, Y.; Duan, X. Highly Efficient Gate-Tunable Photocurrent Generation in Vertical Heterostructures of Layered Materials. *Nat. Nanotechnol.* **2013**, *8*, 952–958.
- (14) Hou, Y.; Wen, Z.; Cui, S.; Guo, X.; Chen, J. Constructing 2D Porous Graphitic C<sub>3</sub>N<sub>4</sub> Nanosheets/Nitrogen-Doped Graphene/Layered MoS<sub>2</sub> Ternary Nanojunction with Enhanced Photoelectrochemical Activity. *Adv. Mater.* **2013**, *25*, 6291–6297.
- (15) Hong, X.; Kim, J.; Shi, S.; Zhang, Y.; Jin, C.; Sun, Y.; Tongay, S.; Wu, J.; Zhang, Y.; Wang, F. Ultrafast Charge Transfer in Atomically Thin MoS<sub>2</sub>/WS<sub>2</sub> Heterostructures. *Nat. Nanotechnol.* **2014**, *9*, 682–686.
- (16) Yang, H.; Heo, J.; Park, S.; Song, H. J.; Seo, D. H.; Byun, K. E.; Kim, P.; Yoo, I.; Chung, H. J.; Kim, K. Graphene Barristors, a Triode Device with a Gate-controlled Schottky Barrier. *Science* **2012**, *336*, 1140–1143.
- (17) Deng, Y.; Luo, Z.; Conrad, N. J.; Liu, H.; Gong, Y.; Najmaei, S.; Ajayan, P. M.; Lou, J.; Xu, X.; Ye, P. D. Black Phosphorus Monolayer MoS<sub>2</sub> van der Waals Heterojunction p-n Diode. *ACS Nano* **2014**, *8*, 8292–8299.
- (18) Huang, C.; Wu, S.; Sanchez, A. M.; Peters, J. J. P.; Beanland, R.; Ross, J. S.; Rivera, P.; Yao, W.; Cobden, D. H.; Xu, X. Lateral

Heterojunctions within Monolayer MoSe<sub>2</sub>–WSe<sub>2</sub> Semiconductors. *Nat. Mater.* **2014**, *13* (12), 1096–1101.

(19) Kang, J.; Tongay, S.; Zhou, J.; Li, J. B.; Wu, J. Q. Band Offsets and Heterostructures of Two-dimensional Semiconductors. *Appl. Phys. Lett.* **2013**, *102*, 012111.

(20) Tongay, S.; Fan, W.; Kang, J.; Park, J.; Koldemir, U.; Suh, J.; Narang, D. S.; Liu, K.; Ji, J.; Li, J.; Sinclair, R.; Wu, J. Tuning Interlayer Coupling in Large-Area Heterostructures with CVD Grown MoS<sub>2</sub> and WS<sub>2</sub> Monolayers. *Nano Lett.* **2014**, *14*, 3185–3190.

(21) Shi, S. F.; Wang, F. Atomically Thin P–N Junctions. *Nat. Nanotechnol.* **2014**, *9*, 664–665.

(22) Grundmann, M.; Karsthof, R.; von Wenckstern, H. Interface Recombination Current in Type II Heterostructure Bipolar Diodes. *ACS Appl. Mater. Interfaces* **2014**, *6*, 14785–14789.

(23) Furchi, M. M.; Pospischil, A.; Libisch, F.; Burgdörfer, J.; Mueller, T. Photovoltaic Effect in an Electrically Tunable van der Waals Heterojunction. *Nano Lett.* **2014**, *14*, 4785–4791.

(24) Radisavljevic, B.; Radenovic, A.; Brivio, J.; Giacometti, V.; Kis, A. Single-layer MoS<sub>2</sub> Transistors. *Nat. Nanotechnol.* **2011**, *6*, 147–150.

(25) Liu, F.; Shimotani, H.; Shang, H.; Kanagasekaran, T.; Zolyomi, V.; Drummond, N.; Falko, V. I.; Tanigaki, K. High-Sensitivity Photodetectors Based on Multilayer GaTe Flakes. *ACS Nano* **2014**, *8*, 752–760.

(26) Ma, Z.; Hu, Z.; Zhao, X.; Tang, Q.; Wu, D.; Zhou, Z.; Zhang, L. Tunable Band Structures of Heterostructured Bilayers with Transition-Metal Dichalcogenide and MXene Monolayer. *J. Phys. Chem. C* **2014**, *118*, 5593–5599.

(27) Yang, S.; Tongay, S.; Li, Y.; Yue, Q.; Xia, J.; Li, S.; Li, J.; Wei, S. Layer-dependent Electrical and Optoelectronic Responses of ReSe<sub>2</sub> Nanosheet Transistors. *Nanoscale* **2014**, *6*, 7226–7231.

(28) Eda, G.; Yamaguchi, H.; Voiry, D.; Fujita, T.; Chen, M.; Chhowalla, M. Photoluminescence from Chemically Exfoliated MoS<sub>2</sub>. *Nano Lett.* **2011**, *11*, 5111–5116.

(29) Buscema, M.; Groenendijk, D. J.; Steele, G. A.; van der Zant, H. S. J.; Castellanos-Gomez, A. Photovoltaic Effect in Few-layer Black Phosphorus PN Junctions Defined by Local Electrostatic Gating. *Nat. Commun.* **2014**, *5*, 4651.

(30) Huo, N.; Yang, J.; Huang, L.; Wei, Z.; Li, S.; Wei, S.; Li, J. Tunable Polarity Behavior and Self-Driven Photoswitching in p–WSe<sub>2</sub>/n–WS<sub>2</sub> Heterojunctions. *Small* **2015**, *11*, 5430–5438.

(31) Yang, S.; Li, Y.; Wang, X.; Huo, N.; Xia, J.; Li, S.; Li, J. High Performance Few-layer GaS Photodetector and Its Unique Photoresponse in Different Gas Environments. *Nanoscale* **2014**, *6*, 2582.

(32) Jariwala, D.; Sangwan, V. K.; Wu, C.; Prabhumirashi, P. L.; Geier, M. L.; Marks, T. J.; Lauhon, L. J.; Hersam, M. C. Gate-tunable Carbon Nanotube–MoS<sub>2</sub> Heterojunction P–N Diode. *Proc. Natl. Acad. Sci. U. S. A.* **2013**, *110*, 18076–18080.

(33) Wang, Q.; Safdar, M.; Xu, K.; Mirza, M.; Wang, Z.; He, J. Van der Waals Epitaxy and Photoresponse of Hexagonal Tellurium Nanoplates on Flexible Mica Sheets. *ACS Nano* **2014**, *8*, 7497–7505.

(34) Hu, L.; Yan, J.; Liao, M.; Wu, L.; Fang, X. Ultrahigh External Quantum Efficiency from Thin SnO<sub>2</sub> Nanowire Ultraviolet Photodetectors. *Small* **2011**, *7*, 1012–1017.

(35) Li, L.; Wu, P.; Fang, X. S.; Zhai, T. Y.; Dai, L.; Liao, M. Y.; Koide, Y.; Wang, H. Q.; Bando, Y.; Golberg, D. Single-crystalline CdS Nanobelts for Excellent Field-emitters and Ultrahigh Quantum-efficiency Photodetectors. *Adv. Mater.* **2010**, *22*, 3161.

(36) Li, L.; Lee, P. S.; Yan, C.; Zhai, T. Y.; Fang, X. S.; Liao, M. Y.; Koide, Y.; Bando, Y.; Golberg, D. Ultrahigh-Performance Solar-Blind Photodetectors Based on Individual Single-crystalline In<sub>2</sub>Ge<sub>2</sub>O<sub>7</sub> Nanobelts. *Adv. Mater.* **2010**, *22*, 5145.

(37) Hu, P.; Wen, Z.; Wang, L.; Tan, P.; Xiao, K. Synthesis of Few-Layer GaSe Nanosheets for High Performance Photodetectors. *ACS Nano* **2012**, *6*, 5988–5994.

(38) Li, L.; Fang, X. S.; Zhai, T. Y.; Liao, M. Y.; Gautam, U. K.; Wu, X. C.; Koide, Y.; Bando, Y.; Golberg, D. Electrical Transport and High-Performance Photoconductivity in Individual ZrS<sub>2</sub> Nanobelts. *Adv. Mater.* **2010**, *22*, 4151.

(39) Zhai, T. Y.; Ma, Y.; Li, L.; Fang, X. S.; Liao, M. Y.; Koide, Y.; Yao, J. N.; Bando, Y.; Golberg, D. Morphology-tunable In<sub>2</sub>Se<sub>3</sub> Nanostructures with Enhanced Electrical and Photoelectrical Performances via Sulfur Doping. *J. Mater. Chem.* **2010**, *20*, 6630.

(40) Hu, P.; Wang, L.; Yoon, M.; Zhang, J.; Feng, W.; Wang, X.; Wen, Z.; Idrobo, J. C.; Miyamoto, Y.; Geoegean, D. B.; Xiao, K. Highly Responsive Ultrathin GaS Nanosheet Photodetectors on Rigid and Flexible Substrates. *Nano Lett.* **2013**, *13*, 1649–1654.

(41) Law, M.; Kind, H.; Messer, B.; Kim, F.; Yang, P. D. Photochemical Sensing of NO<sub>2</sub> with SnO<sub>2</sub> Nanoribbon Nanosensors at Room Temperature. *Angew. Chem., Int. Ed.* **2002**, *41*, 2405.

(42) Lopez-Sanchez, O.; Llado, E. A.; Koman, V.; Morral, A. F.; Radenovic, A.; Kis, A. Light Generation and Harvesting in a van der Waals Heterostructure. *ACS Nano* **2014**, *8*, 3042–3048.

(43) Wang, F.; Wang, Z.; Xu, K.; Wang, F.; Wang, Q.; Huang, Y.; Yin, L.; He, J. Tunable GaTe–MoS<sub>2</sub> van der Waals p–n Junctions with Novel Optoelectronic Performance. *Nano Lett.* **2015**, *15*, 7558–7566.

(44) Lopez-Sanchez, O.; Lembke, D.; Kayci, M.; Radenovic, A.; Kis, A. Ultrasensitive Photodetectors Based on Monolayer MoS<sub>2</sub>. *Nat. Nanotechnol.* **2013**, *8*, 497–501.

(45) Furchi, M. M.; Polyushkin, D. K.; Pospischil, A.; Mueller, T. Mechanisms of Photoconductivity in Atomically Thin MoS<sub>2</sub>. *Nano Lett.* **2014**, *14*, 6165–6170.